Ballistic and diffuse light detection in confocal and heterodyne imaging systems

M. Kempe and A. Z. Genack

New York State Center for Advanced Technology on Ultrafast Photonics Materials and Applications, Department of Physics, Queens College of the City University of New York, Flushing, New York 11367

W. Rudolph and P. Dorn

Department of Physics and Astronomy, University of New Mexico, Albuquerque, New Mexico 87131

Received April 16, 1996; accepted June 17, 1996; revised manuscript received July 1, 1996

The detection of ballistic and diffuse light in confocal and heterodyne imaging systems in transillumination is studied experimentally and theoretically. We find an optimum pinhole size for ballistic light detection and diffuse light rejection for confocal imaging. The ratio of ballistic and diffuse light is found to be determined primarily by sample parameters and aberrations introduced by the sample. For sample and illumination characteristics that are typical for biomedical imaging, the limits of ballistic light detection in confocal imaging are close to the noise limits of standard detectors. Heterodyne detection with narrow-bandwidth light can extend these limits, depending on the spatial and the temporal coherence properties of the transmitted scattered light. © 1997 Optical Society of America. [S0740-3232(97)03501-1]

1. INTRODUCTION

Diffraction-limited resolution in imaging through turbid media requires the detection of ballistic (unscattered) light and the rejection of most of the scattered light. Efficient methods for accomplishing this goal, including time-resolved techniques and heterodyne detection utilizing broad-bandwidth light, have recently been explored.[1] In particular, the heterodyne technique with broad-bandwidth light has been shown to permit shot-noise-limited imaging in strongly scattering samples[2] with a resolution equivalent to what can be achieved with a confocal microscope in the presence of weak scattering.[3–6] From a practical point of view, however, these methods are not without disadvantages. First, they require bright light sources of high spatial coherence. In most cases they rely on picosecond or femtosecond laser systems. Second, obtaining a high-resolution image requires that the time of flight of photons in the reference arm be matched to the time of flight of the ballistic light. This time is not known *a priori*, and it changes with the scan position of the focus in the object. Apart from the inconvenience of constant readjustment, there is some ambiguity when the depth of focus of the optical system and the coherence length of the light source are comparable. This makes such systems considerably more demanding in terms of equipment and handling than the standard confocal laser scanning microscopes that are widely used in biomedical research.[7] The exploration of methods that use narrow-bandwidth illumination from common cw lasers therefore remains a relevant task. Among these methods are confocal spatial filtering,[8,9] Fourier spatial filtering,[10] polarization modulation,[11,12] and heterodyne detection with narrow-bandwidth light.[13,14]

In this paper we explore the limits of confocal spatial filtering for imaging with ballistic light in transillumination. We investigate the factors that influence the ability of the confocal system to reject scattered light as a function of various experimental parameters. We also address the question of extending the limits of the confocal technique by heterodyne detection with narrow-bandwidth light.

2. EXPERIMENTAL RESULTS

Figure 1 is a schematic diagram of the experimental setup for measuring either the heterodyne or the confocal signal. The beam of a helium–neon laser ($\lambda = 632.8$ nm) is split and recombined in a Mach–Zehnder-type interferometer. One arm contains the sample between two identical focusing lenses ($f = 50$ mm, $a_1 = a_2 = a = 12$ mm). In the second arm the reference beam is Doppler shifted 1 kHz by a loudspeaker. The sample was a rectangular cell divided along the diagonal. One part contained water; the second, a suspension of latex spheres and water. If not stated otherwise, we used latex spheres of 0.480-μm diameter (scattering cross section $\sigma_s = 1.26 \times 10^{-9}$ cm^2 and anisotropy factor $g = 0.81$ according to Mie theory). We can change the total scattering density without changing the overall optical parameters (including aberrations) for the ballistic light component by translating the cell transversely. Adjustable diaphragms in front of the objective and the collector lenses are used to control the illumination and the detection apertures of the optical system.

When the confocal response is measured the reference arm is blocked, and the laser beam is modulated by a mechanical chopper. The signal beam is detected by a pinhole–detector combination and a lock-in amplifier. For the heterodyne response the magnitude of the beat signal of the reference and signal light is recorded.

0740-3232/97/010216-08$10.00

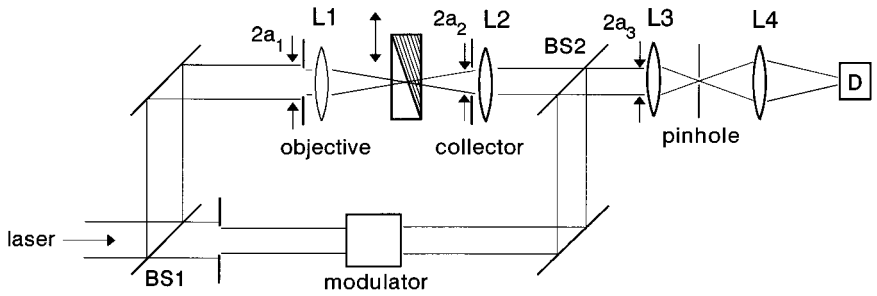

Fig. 1. Experimental setup: BS's beam splitters; a_i, aperture radius of lens L_i; D, detector (photomultiplier tube).

In general, the detected signal consists of a coherent signal from the ballistic light that provides diffraction-limited imaging and an incoherent signal that is due to scattered light. The questions to be addressed are, What is the degree to which scattered light can be suppressed, and what is its dependence on various experimental parameters?

A. Confocal Filtering

Figure 2 shows the confocal signal as a function of the thickness of the scattering medium for two values of the numerical apertures (NA's) of the objective and the collector lenses. In this semilogarithmic plot the initial exponential drop is what one expects for the ballistic signal; from the slope one can deduce the scattering mean-free-path length l_s. The slower decrease for thicker samples results from the detection of diffuse light. It is useful to define a thickness $L_{\max}$ at which the ballistic and diffuse light intensities are equal. Roughly, this is the limit up to which diffraction-limited imaging is feasible. $L_{\max}$ is approximately the sample length at which the measured signal is twice the (theoretical) ballistic signal. The fall-off of the diffuse light suggests a power dependence L^p with $p = -3.1 \pm 0.4$.

The pinhole size, or more precisely the lens–pinhole k-space filter, plays a decisive role in confocal imaging. The essential parameter is the pinhole diameter in optical units $v_p = \pi a_3 d_p/(\lambda f_3)$, where d_p is the geometrical pinhole diameter, f_3 is the focal length, and a_3 is the aperture radius of lens L3. We can change v_p while keeping the illuminating power constant (a_3 = constant) by changing either the diameter of the pinhole d_p or the focal length of the lens f_3. The transmission of the ballistic light component through the pinhole, normalized to the light power incident upon the pinhole, is depicted in curve (a) of Fig. 3 as a function of v_p. Here the scatterer was chosen thin enough to allow us safely to neglect the diffuse light signal. Curve (b) shows the normalized length $L_{\max}$ as a measure of the scattered-light rejection that was determined from plots such as those shown in Fig. 2. The solid curve is a theoretical curve that is explained in Section 3. Obviously, for pinhole sizes $v_p < v_{\text{opt}} \simeq 2$ there is no change in the ability to reject diffuse light. As might be expected, v_{opt} equals the optimum pinhole diameter found for depth discrimination in confocal imaging.[15] Increasing the pinhole diameter beyond v_{opt} increases the relative contribution of diffuse light and reduces the achievable resolution.

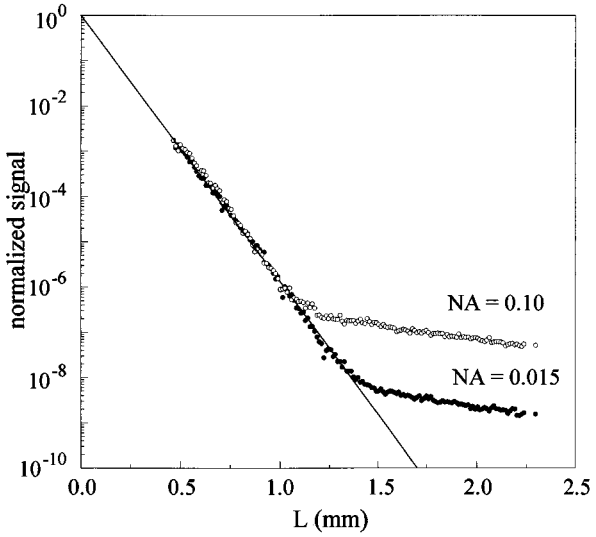

Fig. 2. Semilogarithmic plot of the signal as a function of sample thickness for a suspension with $l_s = 74$ μm. Shown is the signal obtained with a NA of 0.10 for a pinhole with $v_p = 1.24$ and for a NA of 0.015 with $v_p = 1.16$. The solid line is the fit to the part of the curves that exhibits an exponential falloff.

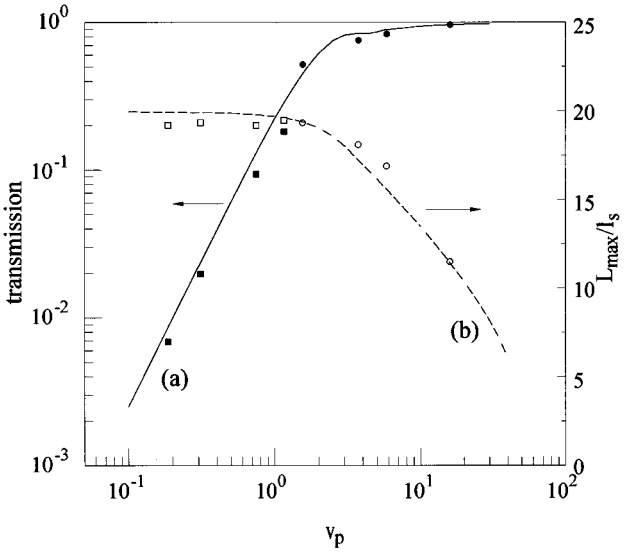

Fig. 3. (a) Log–log plot of the pinhole transmission for ballistic light (at $L = 0.47$ mm) and (b) semilogarithmic plot of the maximum sample thickness $L_{\max}$ as a function of the normalized pinhole size. The NA is 0.015. The suspension had a scattering mean free path of 74 μm. The pinhole had a diameter of 10 μm (squares) and 50 μm (circles), respectively. The focal length of lens L3 was varied from 32 to 200 mm. The solid and the dashed curves result from calculations explained in the text.

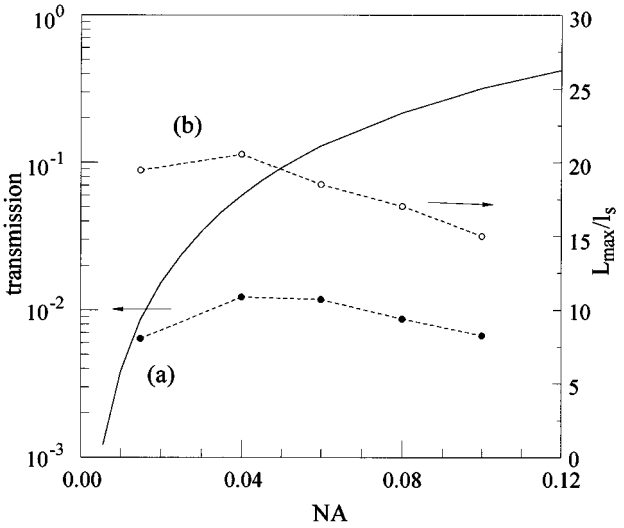

Fig. 4. Semilogarithmic plots of (a) the pinhole transmission for ballistic light (at $L = 0.47$ mm) and (b) the maximum sample thickness L_{max} as a function of the NA. We increased the NA by increasing the beam radius a. The solid curve is the theoretical curve of the pinhole transmission in the absence of aberrations. The dashed lines connecting the measured points are only guides for the eye.

To study the effect of the NA we varied the objective and the collector apertures. To exclude the effects of the pinhole described above we kept $v_p < 1.5$. The pinhole transmission of the ballistic light component as a function of the NA is shown in curve (a) of Fig. 4. Again, the sample was thin enough to allow us to neglect diffuse light. The drop in the relative transmission with increasing NA can be attributed to aberrations of the sample. In this case L_{max}/l_s decreases with increased NA; see curve (b) of Fig. 4. The same arguments explain the differences observed in Fig. 2 for the two NA values. In Section 3 we show that aberrations do not affect the diffuse light. Because the detectable ballistic light is expected to be a function of L/l_s only in the absence of aberrations, we can estimate how L_{max}/l_s would vary as a function of the NA without aberrations. We find the confocal results from Fig. 4 corrected in this manner to be approximately independent of the NA.

Unlike the ballistic light, which depends only on L/l_s, the diffuse component also exhibits an explicit dependence on the geometrical sample thickness L. Therefore we expect that L_{max}/l_s is a function of l_s. Figure 5 shows the experimental results. We varied the scattering mean free path l_s by changing the concentration of the scatterers while keeping all the other experimental parameters constant. The measurement point at $l_s = 8$ μm was obtained by use of a thin alumina wedge as a sample. The transport mean free path l of this wedge was determined from total transmission measurements to be $l = 45$ μm. The anisotropy factor is $g = 1 - l_s/l = 0.82$ and is thus comparable with that of the latex suspension. A weak dependence of L_{max} on l_s can be seen in Fig. 5.

All the previous measurements were performed with the back of the sample in the focal plane of the collector lens. Figure 6 shows the behavior of the diffuse light detected as the back of the alumina sample is moved out of the focal plane. The falloff is slow on a length scale comparable with the sample thickness.

B. Heterodyne Filtering

To measure the heterodyne response we detected the interference signal of the reference field and the field transmitted through the sample. We determined the modulation amplitude by amplifying and rectifying the interference signal. Figure 7 compares the confocal with the heterodyne signal as a function of the thickness of the scattering suspension for a NA of 0.25. For $L < 0.96$ mm the confocal signal drops twice as fast as the heterodyne signal, as is expected for the ballistic light component. Up to the sample thickness of $L \approx 1.3$ mm ($\approx 21.5 l_s$) the

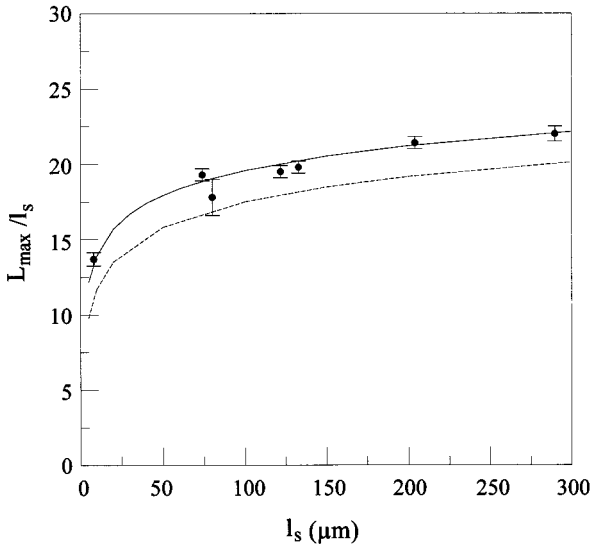

Fig. 5. Maximum sample thickness L_{max}/l_s as a function of l_s. The theoretical results (solid and dashed curves) are explained in the text.

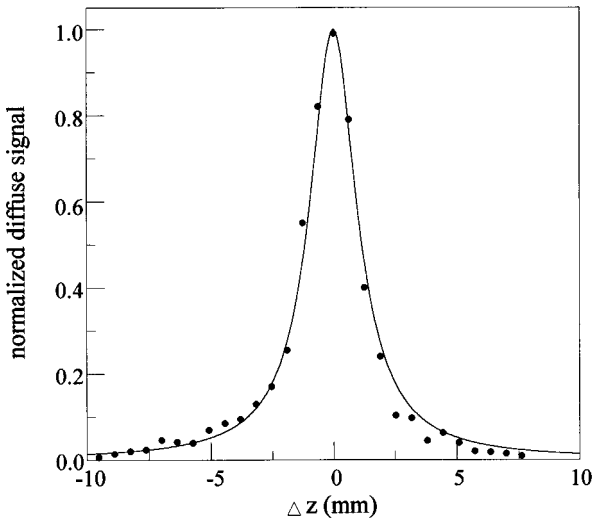

Fig. 6. Diffuse-light signal as a function of the distance between the back surface of the sample and the focal plane of the collector lens. The sample was alumina with a scattering mean free path of $l_s = 8$ μm and a thickness of 70 μm. The result according to Eq. (18) is shown as a solid curve.

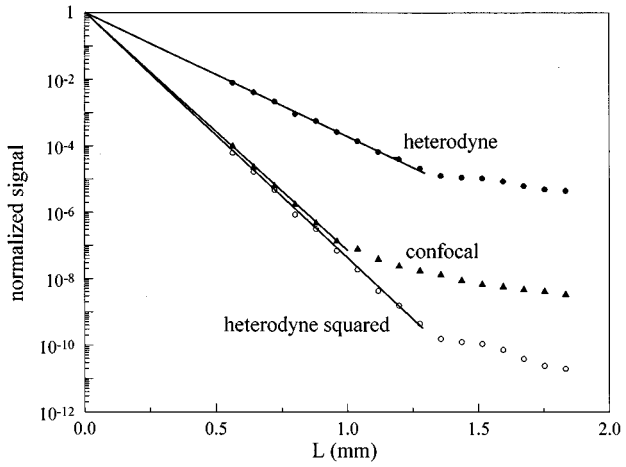

Fig. 7. Semilogarithmic plot of the normalized confocal and heterodyne signals. In these measurements latex spheres with diameters of 135 μm ($\sigma_s = 3.10 \times 10^{-12}$ cm^2, $g = 0.14$ according to Mie theory) were used. The power in the reference arm was 100 μW, and the power incident upon the sample was 1 mW.

heterodyne signal appears to be due to ballistic light. In contrast, the confocal signal is dominated by diffuse light for a sample thickness $L > 0.96$ mm ($\approx 16 l_s$). Because the ballistic light is affected by aberration to the same extent in the confocal and the heterodyne setups, the superior performance of the heterodyne system suggests a better filtering of scattered light. Further experiments, for example, the measurement of the achievable imaging resolution and of the coherence properties of the light at the sample surface, are necessary to clarify the exact nature of the heterodyne signal at large scattering densities.

3. THEORY AND DISCUSSION

Let us start with some order-of-magnitude estimates of the signal that can be expected in the confocal and heterodyne setups; see Fig. 8(a). The objective is illuminated by a Gaussian beam. In the confocal setup the exit plane of the scattering suspension (assumed to be the position of the focus of the ballistic light) is imaged into the plane of the pinhole with a magnification of one ($d_1 = d_2$). Throughout our analysis we consider equal focal lengths and apertures for objective and collector lenses, that is, $f_1 = f_2 = f$ and $a_1 = a_2 = a_3 = a$, respectively. The diameter of the pinhole d_p matches the beam waist $w = \lambda d_1/a$ of the unscattered light. Assuming no aberrations, the ballistic light reaches the detector essentially without losses other than those introduced by absorption and scattering of the sample. Neglecting absorption, we can write the losses as

$$K_b = \exp(-L/l_s). \tag{1}$$

Throughout this section we use the subscripts b and d to denote the properties of ballistic and diffuse light, respectively. The diffuse (incoherent) light has spread to a circle of radius $s \approx L/2$ at the exit plane of the scattering medium. The loss factor of the diffuse light can be approximated as

$$K_d \approx l/L, \tag{2}$$

where the transport mean free path $l = l_s/(1 - g)$ and the anisotropy factor $g = \langle \cos \theta \rangle$ is the averaged cosine of the scattering angle. The diffuse light is imaged onto the plane of the pinhole and is attenuated owing to the finite aperture of the collector lens by a factor $(a/d_1)^2/2$. An additional loss factor is given by the ratio of the pinhole area to the area of the incoherent image on the detector. The total signal measured by the detector is thus

$$\frac{S_{\text{conf}}}{P_0} = \exp(-L/l_s) + 2\lambda^2 \frac{l}{L^3}, \tag{3}$$

where P_0 is the incident power. The second term, which is due to diffuse light, shows the L^{-3} dependence that was observed experimentally. The ratio of ballistic and diffuse signals is

$$R_{bd} \approx \frac{L^2}{2\lambda^2} \frac{L}{l} \exp(-L/l_s). \tag{4}$$

These results suggest that the rejection of diffuse light depends only on the sample properties and is independent of the optical system, notably its NA, if aberrations are neglected.

For the heterodyne signal we need to analyze the correlation of the field from the sample with a coherent plane reference wave that is frequency shifted by ω_m behind the collector lens. The amplitude of the ac heterodyne signal can be written as[16]

$$S_{\text{het}} = \sqrt{Q}\left[\int_D \int_D \mathrm{d}^2\mathbf{r}\mathrm{d}^2\mathbf{r}' M_o(\mathbf{r}, \mathbf{r}') M_r{}^*(\mathbf{r}, \mathbf{r}')\right]^{1/2}, \tag{5}$$

where $M_{r/o}$ are the mutual intensities of the reference and the signal waves, respectively; Q is a conversion factor characteristic of the detection system; and $\mathbf{r}$ and $\mathbf{r}'$ are coordinates in the detector plane (area D). We compare the ballistic $S_{\text{het},b}$ and diffuse $S_{\text{het},d}$ heterodyne signals for the case in which the sample (radiating surface) is in the focal plane of the lens. For a rough estimate we

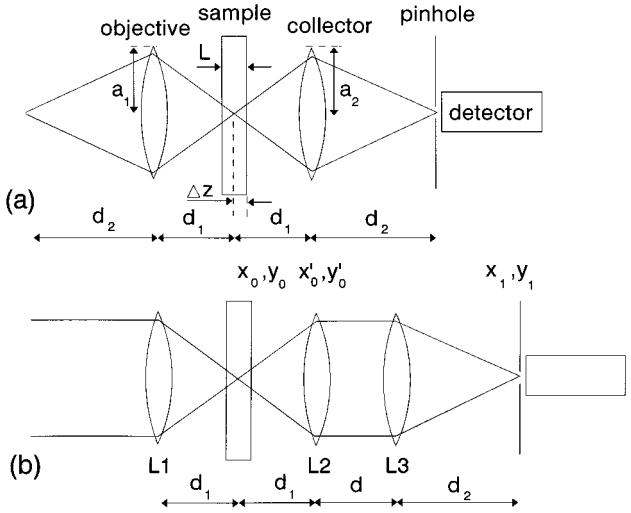

Fig. 8. Geometry of the confocal imaging system (a) with objective and collector lenses only and (b) with a third lens used to focus into the pinhole in front of the detector.

proceed as follows. For the ballistic signal we assume a coherent radiator of uniform intensity in a circular area whose radius corresponds to the first zero of the amplitude point-spread function (PSF) of the collector lens. With this assumption and with the damping factor being taken into account, evaluating Eq. (5) yields

$$S_{\mathrm{het},b} \approx 0.73\sqrt{Q}\sqrt{P_r P_o}\,\exp(-0.5L/l_s), \tag{6}$$

where $P_{r/o}$ are the reference power and the power incident upon the sample, respectively.

For the diffuse light we assume an incoherent source of uniform intensity with area $\pi(L/2)^2$. With the inclusion of the damping factor the heterodyne signal derived from Eq. (5) is

$$S_{\mathrm{het},d} \approx \sqrt{Q}\,\frac{2\lambda}{\pi}\,\frac{1}{L}\sqrt{\frac{l}{L}}\sqrt{P_r P_o}. \tag{7}$$

If the scatterers are nonstationary and fluctuate with a characteristic time τ_c, the heterodyne signal is damped by a factor of $\approx\sqrt{\tau_c/T}$, where T is the integration time of the detection system. This result gives for the ratio of $S_{\mathrm{het},b}$ and $S_{\mathrm{het},d}$

$$R_{\mathrm{het},bd} \approx 0.37\,\frac{\pi L}{\lambda}\sqrt{\frac{L}{l}}\sqrt{\frac{T}{\tau_c}}\exp(-0.5L/l_s). \tag{8}$$

At scattering densities for which the ratio R_{bd} in the confocal setup is approximately unity, the ratio

$$R_{\mathrm{het},bd}(R_{bd}=1) \approx 1.6\sqrt{T/\tau_c}. \tag{9}$$

With correlation times in the microsecond region and integration times in the millisecond region, relation (9) can explain the observed improvement of the heterodyne signal compared with that of the confocal signal.

A more exact treatment is needed to address the effects of homogeneously illuminated lens apertures, which are common in microscopy, as opposed to Gaussian beams and wave aberrations on the imaging and the rejection of scattered light. We base our more rigorous analysis of the confocal system on the scalar, paraxial diffraction theory of wave propagation. This theory describes the propagation of the ballistic (coherent) light through the optical system and the sample. However, it is an adequate description of the propagation of scattered (incoherent) light only outside the sample. Let us consider first the propagation of the scalar fields from the back surface of the scattering medium (coordinates with subscript 0) to the detector plane (coordinates with subscript 1). The coordinates and the variables of the optical system are shown in Fig. 8. If the imaging system is space invariant and exhibits a cylindrical symmetry about the optic axis (z axis), we can write the field amplitude U in the detector plane as

$$U(r_1) = \frac{2\pi^2}{\lambda^2}\int_0^\infty \mathrm{d}r_0 r_0 h(x_1-x_0,\,y_1-y_0)U(r_0), \tag{10}$$

where h is the amplitude PSF of the collector lens. The intensity in the detector plane is then $I(r_1)=|U(r_1)|^2$.

For δ-correlated incoherent fields the intensity in the detector plane becomes[17]

$$I_{\mathrm{inc}}(r_1) = \frac{4\pi^3}{\lambda^2}\int_0^\infty \mathrm{d}r_0 r_0 |h(x_1-x_0,\,y_1-y_0)|^2 I(r_0). \tag{11}$$

For perfectly coherent light the intensity is

$$I_c(r_1) = \frac{4\pi^4}{\lambda^4}\left|\int_0^\infty \mathrm{d}r_0 r_0 h(x_1-x_0,\,y_1-y_0)U(r_0)\right|^2. \tag{12}$$

The amplitude distribution $U(r_0)$ of the ballistic light is

$$U(r_0) = \frac{-j\pi a^2}{\lambda d_1}h(v,\,\Phi)\sqrt{I_0 K_b}, \tag{13}$$

where $v = 2\pi a r_0/\lambda d_1$ is the radius coordinate in the object plane in optical units, Φ is the aberration function,[18] and I_0 is the intensity of light incident upon the objective lens aperture. The aberration function describes the effects of defocus of the back surface of the sample with respect to the focal plane of the collector lens and aberrations in the image performance that are introduced by the sample and the optical system.

The normalized amplitude PSF can be written as

$$h(v,\,\Phi) = 2\exp[-jd_1 v^2\lambda/(4\pi a^2)] \times \int_0^1 \mathrm{d}r r J_0(rv)\exp[-j\Phi(r)], \tag{14}$$

where J_0 is the Bessel function of the first kind and of zeroth order. In the following discussion we consider the two lowest-order monochromatic terms of the aberration function: defocus and primary spherical aberration, $\Phi(r) = ur^2/2 - u(d_1/a)^2 - Ar^4$. $u = 2\pi(a/d_1)^2\Delta z$ is the normalized optical coordinate describing defocus.

Combining Eqs. (12) and (13), we obtain for the total intensity of the ballistic light in the detector plane

$$I_b(v_1) = \frac{\pi^2 {d_1}^2}{4\lambda^2} I_{\mathrm{in}} K_b \times \left|\int_0^\infty \mathrm{d}v\, v h(x_1-x_0,\,y_1-y_0,\,\Phi_b)h(v,\,\Phi_b)\right|^2, \tag{15}$$

with v_1 being the normalized radius coordinate in optical units. Because the overall optical system is normally adjusted in such a way that the ballistic light is in focus at the pinhole, Φ_b contains only the spherical aberration term.

The diffusively transmitted light intensity at the sample surface can be represented by a distribution $I_a f(r_0)$, with $f(0)=1$. Because the ballistic part will be a negligible fraction of the total power transmitted through a random sample, we can write for the total light power $\pi a^2 I_0 K_d = 2\pi I_a \int_0^\infty \mathrm{d}r_0 r_0 f(r_0)$. So far, we have not made any assumptions concerning the properties of the light emerging from the sample surface. However, because we treat its subsequent propagation in the incoherent limit, we require that its spatial coherence extend only over an area λ^2/π. The spatial profile of light transmitted through sufficiently thick samples with $L \geqslant 5l$ has been shown to follow diffusion theory[19] and, therefore, meets the above criterion. We can write I_a

$= 4a^2 I_0 K_d/(L^2 F)$, with $F = 2\pi \int_0^\infty \mathrm{d}r_0 r_0 f(r_0)/[\pi(L/2)^2]$. A good approximation for the intensity distribution of diffuse light is $f(r_0) \approx \exp(-r_0^2/\sigma^2)$, with $\sigma \approx 0.6 \ldots 1L$, depending on the sample thickness and internal reflectivity. In this case, $F \approx 1.5 \ldots 4$. Combining this with Eq. (11), we arrive at

$$I_d(v_1) = \frac{4\pi {d_1}^2}{L^2 F} I_0 K_d \int_0^\infty \mathrm{d}v v f(v) \times |h(x_1 - x_0, y_1 - y_0, \Phi_d)|^2. \quad (16)$$

In confocal imaging systems a pinhole is placed in the detector plane with radius v_p in optical units. The detected light intensity is therefore

$$I_{\mathrm{det}} = \int_0^{v_p} \mathrm{d}v_1 v_1 I_{b,d}(v_1). \quad (17)$$

For an ideal point pinhole Eq. (17) reduces to $I_{\mathrm{det}} = I_{b,d}(0)$. Under this condition, the measured ratio of ballistic and diffuse light becomes

$$R_{bd} = \frac{I_b(0)}{I_d(0)} = \frac{\pi L^2}{16\lambda^2} \frac{K_b}{K_d} F \frac{|\int_0^\infty \mathrm{d}v v h(v, \Phi_b)^2|^2}{\int_0^\infty \mathrm{d}v v f(v) |h(v, \Phi_d)|^2}. \quad (18)$$

For a given sample and optical system, this ratio can be calculated if the aberration functions for ballistic light, i.e., spherical aberration that is due to the sample and the optical system, $\Phi_b = -A_b r^4$, and for diffusive light, spherical aberration that is due to the optical system and defocus, $\Phi_d = ur^2/2 - u(d_1/a)^2 - A_d r^4$, are known.

If the distribution of diffuse light at the exit plane of the sample, $f(v)$, is much broader than the PSF of the collector lens, $|h(v, \Phi_d)|^2$, which will often be the case, the integral in the denominator of Eq. (18) is a constant, independent of any aberrations. In this case, aberrations introduced by the sample affect only the ballistic light and lower the ratio R_{bd}.

With K_b and K_d from relations (1) and (2), assuming that $F = 4$, and for the limiting case of no aberrations, Eq. (18) becomes

$$R_{bd} = \frac{\pi L^2}{2\lambda^2} \frac{L}{l} \exp(-L/l_s). \quad (19)$$

Apart from a factor of π, this result is identical to that obtained from the estimate [cf. Eq. (3)]. The NA of the optical system enters into the more general expression (18) because spherical aberration increases with NA and if the distribution of diffuse light on the back of the sample is not much broader than the PSF. Both effects lead to a decrease of R_{bd} with increased NA. The spherical aberration will usually be of greater relevance.

The sample thickness $L_{\max}$ at which the diffuse light equals the ballistic light can be obtained by solution of the equation $R_{bd}(L_{\max}) = 1$. The dashed curve in Fig. 5 shows the result of the evaluation of Eq. (19). $L_{\max}$ increases approximately logarithmically with l_s. A better agreement with the experimental results is obtained for $F = 8$ (solid curve), indicating a broader than expected spreading of the diffuse light on the sample's surface.

The finite width of the distribution of the diffuse light also becomes relevant if the PSF broadens, as is the case for large Δz. In general, this effect is important only if $\Delta z > L$. The evaluation of Eq. (16) as a function of Δz for $\sigma = \sqrt{2}L$ (which follows from $F = 8$) is shown in Fig. 6 and agrees well with the experimental results.

From our considerations we expect $L_{\max}$ to be $\sim 20 l_s$ in the absence of aberrations for the sample parameters typically encountered in biomedical imaging. At this sample thickness the detected signal is close to the noise limit of standard detection. For a photodiode, the noise-equivalent power is of the order of 10^{-12} W/$\sqrt{\mathrm{Hz}}$. Assuming a signal-to-noise ratio of 10 and an integration time of 10 ms, the detectable light power is 10^{-10} W. The corresponding power for a typical photomultiplier tube is 10^{-13} W. With an incident light power of 10 mW, the limit of detection would be reached for $L/l_s = 18$ (25) if a photodiode (photomultiplier tube) were used. This fact supports the hypothesis that in many circumstances the confocal system is limited by too small a signal rather than by an insufficient ability to reject diffuse light.[14]

In practice, one often uses an additional lens to focus into the detector; see Fig. 8(b). This arrangement allows one to optimize the pinhole size v_p independently of the lenses used for imaging. The question arises whether this system differs from that depicted in Fig. 8(a), which we have discussed in terms of its ability to reject diffuse light. Let us compare the propagation of a coherent and an incoherent field, which fill the aperture of the collector lens, from the lens to the detector plane. Instead of having a source of light on the sample as before, we now consider the collector lens aperture as a source. Using expressions (11) and (12) with a uniform intensity across the area of the aperture, I^c and I^i, and considering the case of a point pinhole, we obtain

$$\frac{I_c(0)}{I_{\mathrm{inc}}(0)} = \frac{\pi}{\lambda^2} \frac{I^c}{I^i} \frac{\left| \int_0^a \mathrm{d}r_0' r_0' h(r_0', u) \right|^2}{\int_0^a \mathrm{d}r_0' r_0' |h(r_0', u)|^2} = \frac{\pi a^2}{\lambda^2 u^2} \frac{I^c}{I^i} \frac{\left| \int_0^u \mathrm{d}v v h(v, u) \right|^2}{\int_0^u \mathrm{d}v v |h(v, u)|^2}, \quad (20)$$

where, because $f_3 = d_2$, $u = 2\pi a^2/\lambda d$, which equals the aperture radius a in optical units. Using the amplitude PSF from Eq. (14) without spherical aberration, we can finally write

$$\frac{I_c(0)}{I_{ic}(0)} = \frac{\pi a^2}{\lambda^2 u^2} \frac{I^c}{I^i} \times \frac{\left| \int_0^u \mathrm{d}v v \int_0^1 \mathrm{d}r r J_0(rv) \exp\{-ju/2[r^2 + (v/u)^2]\} \right|^2}{\int_0^u \mathrm{d}v v \left| \int_0^1 \mathrm{d}r r J_0(rv) \exp(-jur^2/2) \right|^2}. \quad (21)$$

This ratio is depicted in Fig. 9. It is essentially independent of u and, consequently, independent of d. This re-

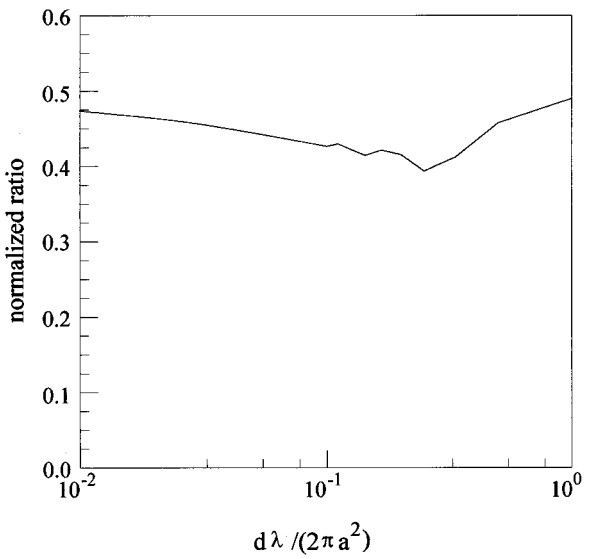

Fig. 9. Calculated normalized ratio of ballistic to diffuse light as a function of the normalized distance between the collector lens and the lens focusing into the pinhole.

sult reflects the fact that the more efficient collection of diffuse light as d decreases is offset by the less efficient imaging of this light onto the pinhole. We verified this experimentally by measuring $L_{\max}$ for the alumina wedge for various separations d of lenses L2 and L3. For distances between $d = 10$ cm and $d = 50$ cm (u between 100 and 20) we found values of $L_{\max}/l_s$ ranging from 13.7 $\pm$ 0.2 to 14.2 $\pm$ 0.5, supporting our conclusions.

Finally, we want to address the question of finite pinhole size. If the diffuse light is homogeneously distributed across the pinhole, its transmission through the pinhole is proportional to the pinhole area. In contrast, the normalized transmission of the ballistic light in the absence of aberrations is $T = 1 - J_0(v_p)^2 - J_1(v_p)^2$.[18] This function is shown as solid curves in Figs. 3 and 4. With everything else kept constant, the ratio of ballistic and diffuse light will, under this condition, change with the pinhole radius as $4T/{v_p}^2$. This factor modifies the ratio R_{bd} as given in Eq. (19) for the case of finite pinhole sizes. The solution of this modified equation for $L_{\max}$ with $F = 8$ is shown in Fig. 3 as a dashed curve. It agrees well with the experimental results.

4. CONCLUSIONS

Confocal spatial filtering is an efficient method for ballistic imaging in transillumination. A pinhole size of 2 in optical units ensures optimum rejection of diffuse light. Because 60% of the unaberrated ballistic beam incident upon such a pinhole is transmitted and detected, a larger pinhole area cannot significantly increase the ballistic signal but does increase the diffuse signal proportionately. Aberrations as introduced by the sample reduce the ballistic light transmitted through the pinhole and, therefore, limit the ballistic imaging capabilities of a confocal imaging system. In the absence of aberrations, ballistic imaging in scattering media is possible for sample and illumination parameters often encountered in biomedical imaging up to sample thicknesses of typically $20l_s$.

The results presented in this paper were obtained for homogeneously scattering samples. Biomedical samples are, however, mostly inhomogeneous. In transillumination the essential characteristics of the scattered light with respect to our analysis, the total transmission, the spatial incoherence, and the intensity distribution at the back side of the sample, are expected to be fairly insensitive to small-scale inhomogeneities. Absorption, if distributed throughout the sample, will support the discrimination of ballistic against diffuse light because of the diffuse light's stronger absorption.

The situation is quite different for reflection geometry. Sample inhomogeneities do strongly affect the reflected diffuse light. In many circumstances the imaging signal comprises light backscattered from the focal region. Because the extent of the focal region is determined by the NA as well as by the pinhole size, there might exist a trade-off among signal size, resolution, and diffuse light rejection. In general, the backscattered light from the sample will be a mixture of light with various degrees of coherence. This makes the analysis of the reflection mode of imaging considerably more complicated than can be accounted for in the model presented in this paper. Monte Carlo simulations[20] and a single-scattering diffraction theory[14] have, for instance, found a diffuse light rejection that improves with the square of the NA. In many biomedical samples, confocal imaging in reflection will be limited to depths of less than a few hundred micrometers.

We have shown that heterodyne detection with narrow-bandwidth light can improve the diffuse light rejection of the confocal setup in transillumination. Further investigations are needed to explore the resolution of the heterodyne technique in the region of transition from ballistic to diffuse light detection. Our experiments indicate that the capabilities of confocal imaging that come close to the detector noise limits can, under certain conditions, be extended up to the shot-noise limit for ballistic light.

ACKNOWLEDGMENTS

We thank Jeffrey Wong for support in performing the confocal measurements and Audra Rice for help in setting up the heterodyne experiment. This project was supported by a National Science Foundation grant and by the W. M. Keck Foundation.

REFERENCES

1. R. R. Alfano, ed., *Advances in Optical Imaging and Photon Migration*, Vol. 21 of OSA Proceedings Series (Optical Society of America, Washington, DC, 1994).
2. M. R. Hee, J. A. Izatt, J. M. Jacobson, J. G. Fujimoto, and E. A. Swanson, "Femtosecond transillumination optical coherence tomography," Opt. Lett. **18**, 950–952 (1993).
3. J. M. Schmitt, A. Knuettel, and M. Yadlowsky, "Interferometric versus confocal techniques for imaging microstructures in turbid biological media," in *Advances in Laser and Light Spectroscopy to Diagnose Cancer and Other Diseases*, R. R. Alfano, ed., Proc. SPIE **2135**, 251–262 (1994).
4. J. A. Izatt, M. R. Hee, G. M. Owen, E. A. Swanson, and J. G.

Fujimoto, "Optical coherence microscopy in scattering media," Opt. Lett. **19**, 590–592 (1994).
5. M. Kempe and W. Rudolph, "Scanning microscopy through thick layers based on linear correlation," Opt. Lett. **19**, 1919–1921 (1994).
6. M. Kempe and W. Rudolph, "Analysis of heterodyne laser scanning microscopy for illumination with broad bandwidth light," J. Mod. Opt. (to be published).
7. J. P. Pawley, ed., *Handbook of Biological Confocal Microscopy* (Plenum, New York, 1990).
8. T. Wilson and C. J. R. Sheppard, *Theory and Practice of Scanning Optical Microscopy* (Academic, London, 1984).
9. T. Wilson, ed., *Confocal Microscopy* (Academic, London, 1991).
10. Q. Z. Wang, X. Liang, L. Wang, P. P. Ho, and R. R. Alfano, "Fourier spatial filter acts as temporal gate for light propagation through a turbid medium," Opt. Lett. **20**, 1498–1500 (1995).
11. H. Horinaka, K. Hashimoto, K. Wada, Y. Cho, and M. Osawa, "Extraction of quasistraightforward-propagating photons from diffused light transmitted through a scattering medium by polarization modulation," Opt. Lett. **20**, 1501–1503 (1995).
12. S. G. Demos and R. R. Alfano, "Temporal gating in highly scattering media by the degree of optical polarization," Opt. Lett. **21**, 161–163 (1996).
13. K. P. Chan, M. Yamada, B. Devaraj, and H. Inaba, "Optical imaging through highly scattering media by use of heterodyne detection in the 1.3-m wavelength region," Opt. Lett. **20**, 492–494 (1995).
14. M. Kempe, W. Rudolph, and E. Welsch, "Comparative study of confocal and heterodyne microscopy for imaging through scattering media," J. Opt. Soc. Am. A **13**, 46–52 (1996).
15. C. J. R. Sheppard and T. Wilson, "Image formation in scanning microscopes with partially coherent source and detector," Opt. Acta **25**, 315–325 (1978).
16. R. G. Frehlich and M. K. Kavaya, "Coherent laser radar performance for general atmospheric refractive turbulence," Appl. Opt. **30**, 5325–5352 (1991).
17. J. W. Goodman, *Statistical Optics* (Wiley, New York, 1985).
18. M. Born and E. Wolf, *Principles of Optics* (Pergamon, London, 1989).
19. J. H. Li, A. A. Lisyansky, T. D. Cheung, D. Livdan, and A. Z. Genack, "Transmission and surface intensity profiles in random media," Europhys. Lett. **22**, 675–680 (1993).
20. J. M. Schmitt, A. Knuettel, and M. Yadlowsky, "Confocal microscopy in turbid media," J. Opt. Soc. Am. A **11**, 2226–2235 (1994).